Lab on a Chip

PAPER

View Article Online
View Journal

Cite this: DOI: 10.1039/c9lc00748b

Microelectrofluidic probe for sequential cell separation and patterning†

Ayoola T. Brimmo,[ab] Anoop Menachery[a] and Mohammad A. Qasaimeh *[ab]

Cell separation and patterning are of interest to several biological and medical applications including rare cell isolation and co-culture models. Numerous microfluidic devices have been used for cell separation and patterning, however, the typical closed channel configuration comes with challenges and limitations. Here, we report a dielectrophoresis (DEP) enabled microelectrofluidic probe (MeFP) for sequentially separating and patterning of mammalian cells in an open microfluidic system. The MeFP is a microfluidic probe with injection and aspiration apertures, integrated with an array of micro-hump electrodes on its tip. Aligning the MeFP parallel, and in close proximity, to a conductive substrate forms a vertical pin-plate electrode configuration that allows for an integration of DEP forces within the hydrodynamic flow confinement. Upon confining a heterogeneous cell suspension in the gap between the MeFP and the substrate, target cells are selectively captured on the micro-hump electrodes using positive DEP forces, and then deposited on the substrate in defined patterns. Characterization of the MeFP showed an increase in cell-capture efficiency when the MeFP is of a higher microfluidic multipole configuration. Separation of cancer cells from T lymphocytes was demonstrated with capture purity as high as 89.6%. Deposited patterns of isolated cells match the numerically calculated particle trajectories of the evaluated microfluidic multipoles configurations. By adjusting the flow configuration of the MeFP, we show that the patterned co-culture of two different cell types can be dynamically controlled for homotypic and heterotypic cell interaction studies. This work presents a multifunctional microfluidic tool that bio-fabricates selective multicellular patterns directly on an open substrate without the need for confined conduits.

Received 29th July 2019,
Accepted 18th October 2019

DOI: 10.1039/c9lc00748b

rsc.li/loc

Introduction

Cell isolation and manipulation are central to many biomedical applications[1] and have been of interest to the microfluidics community since the early days.[2] The capability to separate specific cells from a heterogeneous population has served as a major drive for advanced studies at the single cell resolution.[3,4] This in-turn has delivered ground breaking capabilities in the fields of cell differentiation,[5] drug screening,[6] and tissue engineering.[7] Besides decoupling the heterogeneity in cell populations, cell isolation and manipulation techniques also offer the capability to position cells with controlled placements that permit a deeper understanding of cell–cell interactions.[8] In tissue engineering, these interactions play an important role in regulating functions and fate of tissues and cells.[9] For example, co-culturing of hepatocytes with non-parenchymal cells or fibroblasts has been shown to be critical in stabilizing liver-specific functions.[10,11] This suggests an interdependence between form and function,[12,13] and hence highlights the importance of accurately mimicking the cellular micro-environment for cell and tissue studies.

Early attempts mimicked cellular microenvironment by randomly seeding multiple cell types in culture substrates.[14,15] The strive towards advanced control with single cell resolutions led to the development of micro technologies for patterning multiple cell types with a spatial control that is capable of mimicking tissue-like cellular histoarchitecture.[8,9] Several microfluidic active-force patterning techniques with dynamic and real-time cell manipulation capabilities have been developed.[16–23] They typically utilize magnetic,[16] optical,[17] hydrodynamic,[18] acoustic[19,20] or electrical[21,22] forces to manipulate cells. The most predominant electrical technique is dielectrophoresis (DEP),[23] which stands out as a label-free and scalable technique for cell manipulation.[21]

DEP enabled microfluidic devices are commonly used as particle sorting tools, but based on their ability to spatially isolate cells, they can also be used to produce cellular patterns with

[a] Engineering Division, New York University Abu Dhabi, Abu Dhabi, United Arab Emirates. E-mail: mohammad.qasaimeh@nyu.edu; Tel: +971 2 628 4165
[b] Department of Mechanical and Aerospace Engineering, New York University, NY, USA

† Electronic supplementary information (ESI) available. See DOI: 10.1039/c9lc00748b

complex tissue-like architecture.[23,24] However, these devices usually use narrow channels to direct cells toward the electrodes, which in-turn represent a challenge for growing patterned cells. The channel environment is a diversion from the conventional open cell culture environment and not suitable for long-term cell growth and proliferation, given its restrictive architecture for nutrient, gas, and waste exchange. Furthermore, since the pattern is predefined by channel geometry and the microelectrode's position, there is a shape and size limitation to the resulting patterns – requiring a revamp of the device to adjust the patterned constructs.[25]

To date, no existing tool can separate and pattern cells using DEP forces within an open "channel-less" microfluidic system. Hence, the capability to selectively and dynamically produce cell micro-patterns on a flat and open substrate is still missing. This work presents the microelectrofluidic probe (MeFP), which builds on the hydrodynamic flow confinement (HFC) concept of the microfluidic probe (MFP).[26] The MeFP integrates array of microelectrodes within its tip for DEP-based cell manipulation. As cell suspension flows between the MeFP tip and the substrate, cells of interest are selectively immobilized on the electrodes using positive DEP forces, and subsequently deposited on the substrate in defined micro patterns. Using different microfluidic multipoles configurations,[27–29] the MeFP can achieve high cell separation purity and cells can be patterned in a dynamic and controlled manner with co-culture capabilities. This results in a multifunctional electro-fluidic tool for cell separation, manipulation and patterning directly on flat conductive substrates without the need of physical microchannels.

Materials and method

MeFP fabrication, assembly, and operation

Designs of the MeFP were created on a commercial CAD software (SolidWorks) and the devices were fabricated using a digital light processing (DLP) projector-based stereolithographic (SLA) 3D printer with a XY resolution of 25 μm (Solus DLP, Junction3D, Santa Clarita, CA, USA). The MeFP's apertures were fabricated with a 250 μm diameter and the array of micro-hump electrodes were fabricated with 30 μm height and 180 μm center–center spacing. The commercially available SolusProto resin (Junction3D, Santa Clarita, CA, USA) was utilized. Upon printing, the chip and all apertures were rinsed thoroughly with ethanol, dried with an air gun, and cured in a UV flood light curing system (EnvisionTEC GmbH, Gladbeck, Germany) for 20 minutes. Electrical wires were cold-soldered to the MeFP and ITO coated glass slide (8–12 Ω $sq.^{-1}$, Sigma Aldrich, Saint-Louis, USA) using silver conductive epoxy (M.G Chemicals Limited, Ontario, Canada). To ensure sterility, the chips were subsequently soaked in ethanol for 12 hours, rinsed with DI water and UV cured for an additional 20 minutes. The MeFP chips were made conductive by sputtering gold on the entire surface (Cressington Sputter Coater, Ted Peller, CA, USA) until a surface resistivity of 1 Ω $sq.^{-1}$ is attained.

The pin-plate electrode setup consisting of the MeFP and ITO coated glass slide is established by affixing the MeFP to a 3D printed probe holder (Dimensions SST 1200es 3D Printer, Stratasys, Minnesota, US) and precisely positioning it above the ITO coated glass located on the stage of an inverted microscope using a XYZ micro positioner stage (X-LRM, Zaber, Vancouver, Canada). A more detailed description of this setup is available in our previous work.[30] The other ends of the electrical wires were connected to a function generator (Agilent 33521A, Agilent Scientific Instruments, California, USA) where the sinusoidal waveform of 10 MHz and varying magnitude were induced. A high-power amplifier (ZHL-5W-1, Mini Circuits New York, USA) was used to attain voltages greater than 10 V.

To characterize the isolation efficiency of different MeFP configurations, cells were fluorescently labelled (as described in the cell culture section below), loaded into syringes, and injected through the respective apertures using the neMESYS high precision syringe pump (CETONI, Korbußen, Germany). For all configurations and flow rates, the HFC was activated for 30 seconds and the capture efficiency was estimated as the fraction of injected cells that were isolated at the tip of the electrodes during that period. HFCs were visualized using the Epi-fluorescence inverted ECLIPSE Ti microscope (NIKON, Tokyo, Japan), and images were captured using the DS-Qi2 camera (NIKON). Cell counting was performed by a manual inspection of each frame of the acquired video using a video processing software (Windows Movie Maker, Windows).

Cell culture, viability and density

HeLa and MCF-7 cells (ATCC, VA, USA) were cultured in sterile Petri Dishes (Thermo Scientific) in Dulbecco's modified Eagle medium (DMEM) supplemented with 10% fetal bovine serum (FBS), 100 U mL^{-1} penicillin, 100 μg mL^{-1} streptomycin and 0.2 mM L-glutamine (Invitrogen, MA) at 37 °C and 5% CO_2. Prior to the experiments, the cells were dissociated from the culture dish using trypLE Express (Gibco, Thermo Scientific) and suspended in DMEM for neutralization. T-lymphocytes were cultured in a similar setup but in Roswell Park Memorial Institute (RPMI) medium supplemented with 10% fetal bovine serum (FBS), 100 U mL^{-1} penicillin, 100 μg mL^{-1} streptomycin and 0.2 mM L-glutamine (Invitrogen, MA) at 37 °C and 5% CO_2. Centrifugation at 900 rpm for 5 minutes (Eppendorf Centrifuge 5810, Sigma Aldrich, Saint-Louis, USA) was used to purify cells in pellet. The cells were then washed twice with DEP buffer of 10 mS m^{-1} conductivity and a pH of 7.4. The DEP buffer solution was prepared by mixing (magnetic stirrer) 95 g sucrose, 0.1 g dextrose, and 3 mL 1 M HEPES solution in 950 mL of DI water, and then adjusting the pH and conductivity with 1 M NaOH and DPBS respectively. 0.2 μm sterile filters and autoclaving were used to ensure sterility of the buffer.

CellTracker® Green BODIPY (Thermo Fisher Scientific) was used to fluorescently label HeLa cells suspended in the

DEP buffer solution (2 μL of 10 mM solution per mL of DEP buffer). For experiments with both HeLa and T-lymphocytes, HeLa cells were labeled with CellTracker® RED CMPTX (Thermo Fisher Scientific) and T-lymphocytes were labeled with the green CellTracker dye. After a CellTracker incubation period of 30 minutes, the density of labelled cells was adjusted to a concentration of 2×10^5 cell per mL then loaded into the glass syringes.

Post cell isolation, cell viability and density examinations were performed by pipetting the released cells into a test tube and diluting to 5×10^5 cells per mL of culture media before seeding equal volumes on sterile glass slide. The glass slides are then placed in a sterile petri dish and stored in an incubator (at 37 °C and 5% CO_2) until the live/dead examination and/or cell count is about to be performed. Cell viability and density was estimated by staining the cultured cells with a Live/Dead viability/cytotoxicity kit for mammalian cells – calcein AM (0.5 μL of 4 mM solution per mL of culture media)/thidium homodimer-1 (2 μL of 2 mM solution per mL of cell media), (Invitrogen, Thermo Scientific).

The cell samples used to evaluate the effect of the 3D printer resin were suspended in the DMEM media, passed through the chip at 5 μL min^{-1} for 20 minutes and then seeded on a sterile glass slide. For low conductivity media cell viability and density studies, the cells were suspended in the low conductivity media for 30 minutes then washed twice in DMEM media before seeding in the sterile glass slide. The cell viability and density studies on the ITO glass slide were carried out by directly seeding cells suspended in DMEM media on an ITO glass slide. All control samples were directly suspended in DMEM media and seeded on a sterile glass slide.

Cell sorting, patterning and co-culture

HeLa (17.1 μm measured diameter) and T-lymphocytes (12.4 μm measured diameter) cells were suspended in DEP buffer (2×10^5 cell per mL of DEP buffer) and fluorescently labelled as described in the previous section. Both cell suspensions were mixed and passed through the injection aperture within the HFC and DEP forces simultaneously held for 30 seconds. Time-lapse videos of flowing cells were taken using the corresponding fluorescent filter cube of the microscope. To estimate individual capture efficiency, manual counting was done frame by frame. For the image representations of the cell pattern, a mixture with a cell density of 5×10^6 cell per mL of DEP buffer was used and the individual images from each filer cubes were combined on ImageJ (GNU Library).

After selectively capturing target cells on the electrodes, and washing out of non-target cells with the aspiration flow, both the HFC and DEP forces are turned off to passively release the cells onto the substrate. The MeFP is slowly withdrawn until a tip-substrate gap of about 5 mm is attained. This gap permits X–Y translation of the MeFP to another target spot on the glass slide without interfering with the previously deposited pattern. For co-culture applications, HeLa was stained with a red dye while MCF-7 was stained with a green dye. Different streams are then injected in the respective injection apertures to achieve patterns of different cells in co-culture.

Temperature measurements

Voltage dependent temperature measurements were collected by pointing an infrared camera (Flir, Tester UK) at the area of the glass slide where DEP voltages are being applied.

Numerical and analytical computations

The 3D numerical models of the MeFP's fluid flow were developed using a commercial finite element solver (COMSOL Multiphysics® v.5.2. COMSOL AB, Stockcholm, Sweden). The solutions were obtained using an iterative and stationary solver to compute the coupled Navier–Stokes and convection–diffusion equations, and an iterative solver to compute the continuity equation for the electrical potential. MeFPs were modeled as circular surfaces with inlets and outlets ports, and an array of micro-hump shape protrusions corresponding to fabricated dimensions of the apertures and imbedded electrodes respectively. The injected and immersion fluids were considered as water with a density of 998.2 kg m^{-3} and a dynamic viscosity of 0.001 N s m^{-2}.

In calculating the deposition time using eqn (5), the following values were used: the gravitational constant (9.81 m s^{-1}), radius and density of HeLa (8.5 μm, 1035.7 kg m^{-3}),[31] density and dynamic viscosity of the medium (997 kg m^{-3}, 8.90×10^{-4} Pa s). Shear stress is calculated using eqn (2) with the following values: shear area ($4\pi r^2$), dynamic viscosity of the medium (8.90×10^{-4} Pa s), viscous flow velocity (maximum color band values in Fig. S1†), velocity of cell at capture (0), dimensionless wall effect factor (1 – no translational motion of cell).[32]

Frequency dependent CM functions of MCF-7, HeLa and T-lymphocyte cells were calculated using MATLAB, based on the two-shell model.[33,34] The membrane capacitance (C_m) is used to determine the permittivity of the membrane based on the presence of microvilli and membrane folds, which can be approximated by the expression:[24]

$$C_m = \frac{\sqrt{2}}{2\pi R f_{cr}} \sigma_e$$

In this equation, f_{cr} is the cross-over frequency, σ_e is the conductivity of the suspending medium and R is the cell radius. Based on this equation, we obtain a membrane capacitance of 13.4 mF m^{-2}, 17.6 mF m^{-2} and 10 mF m^{-2} for MCF-7, HeLa and T cells respectively.

Results

Microelectrofluidic probe

The MeFP builds on the MFP technology that confines fluid above a substrate, in the absence of microfluidic channels, based on the HFC concept.[26] The HFC is generated by

forming a quasi-2D stokes flow between two parallel flat plates separated by a small gap, and has been previously demonstrated in the microfluidic dipole (MD),[29] quadrupole (MQ)[27] and multipole (MM)[28] configurations. By integrating an array of micro hump electrodes on the tip of the MFP, we introduce the MeFP technology that produces electrical forces (*i.e.* DEP) within the HFC. This facilitates selective isolation of cells of interest from a suspension of heterogeneous cells, as they flow from the injection to the aspiration aperture (Fig. 1a (i)).

The theory behind selective cell isolation on the micro humps is based on balancing the competing DEP, viscous flow, and gravitational forces acting on the cell (modelled as a spherical particle). The DEP force is given by:[23]

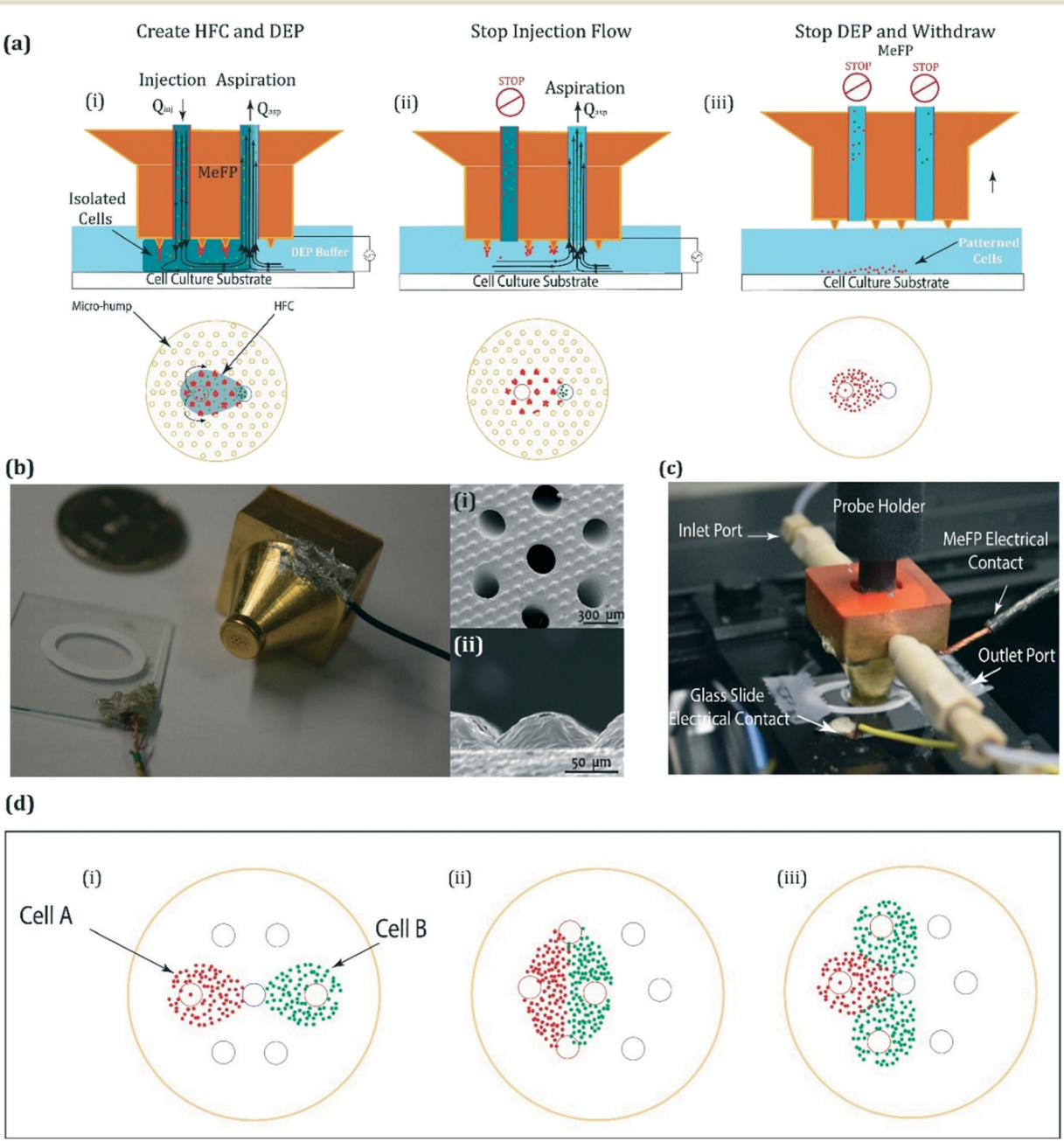

Fig. 1 Working concept of the MeFP for sequential cell separation and patterning. (a) Schematic showing the operational principle of the MeFP. (i) Simultaneous creation of the HFC and DEP forces to selectively isolate target cells (red) from the HFC's flow streams of multiple cells (red and green). (ii) Continuing the aspiration flow after turning off the injection flow to completely pull out the non-isolated cells (green). (iii) Turning off the DEP forces and aspiration flow to deposit target cells (red) on the substrate in a pattern that matches the HFC's shape. (b) Gold coated MeFP and ITO coated glass slide with electrical contacts. Inset. SEM images of (i) microfluidic apertures and (ii) side view of the hump-shaped electrodes. (c) Experimental setup with the MeFP and glass slide in the pin-plate electrode configuration atop an inverted microscope. (d) Configurable co-culture patterns of the microfluidic multipoles. (i) Co-culture with two cell pattern and minimum patterns contacts. (ii) Co-culture with two cell patterns with contact. (iii) Co-culture with three cell patterns in contact.

$$\vec{F}_{\mathrm{DEP}} = 2\pi r^3 \varepsilon_{\mathrm{m}} \mathrm{Re}\left\{\frac{\varepsilon_{\mathrm{p}}^*(\omega) - \varepsilon_{\mathrm{m}}^*(\omega)}{\varepsilon_{\mathrm{p}}^*(\omega) + 2\varepsilon_{\mathrm{m}}^*(\omega)}\right\} \nabla |\vec{E}_{\mathrm{rms}}|^2 \quad (1)$$

where $\vec{F}_{\mathrm{DEP}}$ is the DEP force, r is the cell's radius, ε_{m} is the permittivity of the media, $\varepsilon_{\mathrm{m}}^*(\omega)$ and $\varepsilon_{\mathrm{p}}^*(\omega)$ are the complex permittivity of the media and particle respectively $\left(\varepsilon^* = \varepsilon - j\frac{\sigma}{\omega}\right)$, and ∇E_{rms} denotes the electric field gradient. The mathematical expression between the curly brackets is known as the Clausius-Mossotti (CM) function which is proportional to the frequency-dependent complex permittivity of both the particle and the medium.[23,24]

According to Stokes law, the resulting frictional drag imposed on the cell by the viscous flow force is given by:[32,35]

$$\vec{F}_{\mathrm{d}} = 6\pi\mu r(\vec{V} - \vec{v}_{\mathrm{c}}) \quad (2)$$

where μ is the dynamic viscosity, r is the radius of the cell, $\vec{V}$ is the bulk flow velocity, and v_{c} is the cell's velocity.

The gravitational force component can be defined as:

$$\vec{F}_{\mathrm{g}} = \frac{4}{3} g\pi r^3 (\rho_{\mathrm{c}} - \rho_{\mathrm{f}}) \quad (3)$$

where ρ_{c} is the density of the cell, ρ_{f} is the density of the fluid, and g is the gravitational constant. Based on eqn (1), depending on the inherent physiological composition of the cells (represented as complex permittivity dependent CM function in eqn (1)), they will either be attracted to (positive DEP), or repelled from (negative DEP), the high electric-field region – at the tip of the electrodes. Since, the magnitude of the positive or negative DEP forces are dependent on the cube of the particles' radius and the AC frequency dependent permittivity, discrepancies between cell types can be achieved by the difference in $\vec{F}_{\mathrm{DEP}}$ experienced by the cell. However, $\vec{F}_{\mathrm{DEP}}$ has to compete with drag and gravitational forces to immobilize the cell as it flows from the injection to aspiration aperture. By balancing all forces acting on the cell, the condition for capture is when $\vec{F}_{\mathrm{DEP}}$ is greater than the viscous flow and gravitational components:

$$\vec{F}_{\mathrm{DEP}} > \vec{F}_{\mathrm{g}} + 6\pi\mu r(\vec{V}) \quad (4)$$

When both the viscous flow and DEP forces are removed, cells captured on the tip of the electrode are released into a terminal velocity which can be estimated by equating eqn (2) to (3) to obtain:[35]

$$v_t = \frac{\frac{2}{9}(\rho_{\mathrm{c}} - \rho_{\mathrm{f}})}{\mu} g r^2 \quad (5)$$

where ρ_{c} is the density of the cell, ρ_{f} is the density of the fluid, and g is the gravitational constant. By inserting the measured density of single cancer and T lymphocyte cells[31,36] into eqn (5), we estimate that the released cell will take less than 5 s to reach the substrate located 40 μm below. As such, since the pattern in which the target cells are isolated matches the shape of the HFC (see bottom view of Fig. 1a (i)), by allowing the cells to drop under the influence of gravity, this cell pattern can be transferred to the bottom substrate in a few seconds. However, prior to switching off both forces, to completely pull out all of the non-target cells, the aspiration flow must continue for a few seconds after turning off the injection flow of heterogonous cell suspensions (Fig. 1a (ii)). Subsequently, the aspiration flow and the DEP forces are turned off to release the target cells from the electrodes onto the substrate in a predefined pattern (Fig. 1a (iii)).

The MeFP technology takes advantage of our previously developed framework of stereolithographic 3D printing of MFPs,[30] which permits the integration of an array of micro humps on the tip of the device (Fig. 1b) – features that are otherwise very challenging to produce with conventional microfabrication techniques. By forming the stoke flow setup between gold coated MeFP and a bottom glass slide coated with indium tin oxide (ITO) (Fig. 1c), non-uniform electric fields are introduced into the HFC to selectively isolate cells out of the flow streams based on DEP forces. Any multipolar microfluidic probe configurations can then be adopted for dynamic control of the produced cell patterns and the corresponding co-culture environment (Fig. 1d). After achieving the cellular pattern, the substrate can then be placed in an incubator for the growth and proliferation of the patterned cells in a channel-less environment.

Eqn (2) shows that the competing viscous flow force is directly proportional to the stream velocity as the cells are transported from the injection to aspiration aperture. Therefore, at a given applied DEP force, lowering the fluid velocity can enhance the capture efficiency. A direct way of reducing the flow velocity is to reduce mass flow rate but this has an undesirable effect of decreasing the throughput. Based on the mass conservation and continuity equations, flow velocity within the HFC can also be reduced by increasing the number of aspiration apertures, while maintaining the same total mass flow rate and aspiration to injection flow rates ratio. To this effect, three independent microfluidic multipoles configurations were considered while designing the MeFP (Fig. 2a): dipole (1 injection and 1 aspiration apertures), quadrupole (1 injection and 3 aspiration apertures) and heptapole (1 injection and 6 aspiration apertures). For a given throughput, the effect of these configurations on the shape and average velocity within the HFC were examined numerically using the COMSOL Multiphysics modeling software. The well-established tear shape of the microfluidic dipole is evident from the flow stream and velocity profile contours (Fig. 2b(i) and c (i)). For the microfluidic dipole configuration, with an injection flow of 5 μL min^{-1}, flow ratio (defined as the ratio of the total aspiration to inject flow rates) of 3, aperture spacing of 1200 μm and a tip-substrate spacing of 40 μm, the calculated average flow velocity between the apertures is ~13 mm s^{-1}. Using the microfluidic quadrupole configuration where three aspiration apertures are positioned equidistance from the injection aperture (Fig. 2a (ii)) results in a broader HFC footprint (Fig. 2b (ii)) and lower average flow velocity of ~6.9 mm s^{-1} (Fig. 2c (ii)). For the same flow ratio of 3, the velocity

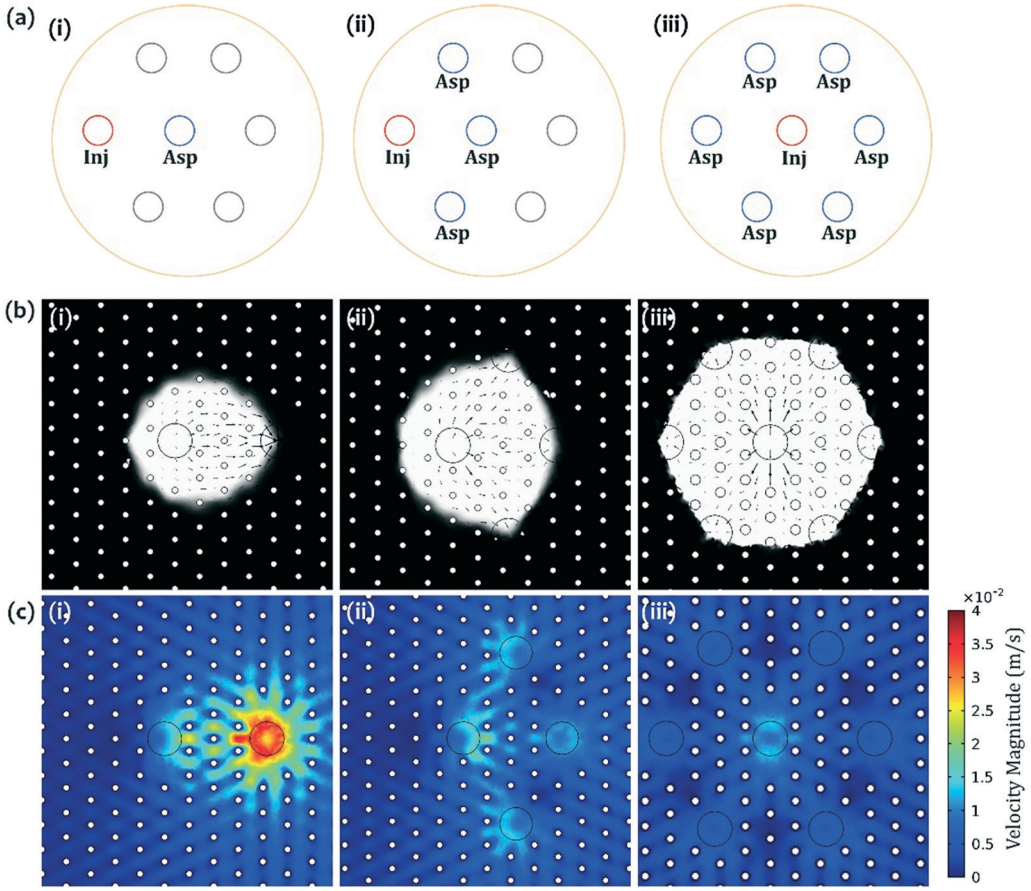

Fig. 2 HFC shape and velocity profiles under the MeFP for different microfluidic multipoles configurations. (a) Schematic showing the MeFP's apertures and applicable configurations for (i) one, (ii) three, and (iii) six aspiration apertures. Blue, red and grey circles represent aspiration, injection and dormant apertures in each frame. (b) HFC shape and flow path for (i) one, (ii) three, and (iii) six aspiration apertures. Injection flow rate is 5 μL min^{-1} and flow rates ratio is 3. All apertures are 250 μm in diameter and spaced at 800 μm center–center. The pattern of small circles in (b) and (c) represent the tip of the electrodes.

within the microfluidic quadrupole configuration is also more uniform (Fig. 2b). By further increasing the aspiration apertures to six, as in the microfluidic heptapole configuration, the shape of the HFC can be more closely controlled and the average velocity can be further reduced (Fig. 2a (iii)). The radially symmetrical configuration ensures a circular HFC shape (Fig. 2b (iii)) while the increase in the number of aspiration apertures resulted in a reduced average flow velocity of ~3.7 mm s^{-1} across the HFC with extremely uniform flow profile except at the vicinity of the aspiration aperture.

The shear stress imposed on the captured cell is also directly proportional to the bulk flow velocity (indicated in eqn (2)). As such, the upper limit of the applicable velocity is bounded by the resulting yield shear stress of the cell. This highlights another advantage of the relatively low velocity profile of the microfluidic heptapole configuration. Considering a relatively high injection flow rate of 20 μL min^{-1}, and the computationally calculated velocity profile of each configuration (Fig. S1†), the resulting maximum shear stress imposed with the microfluidic dipole, quadrupole and heptapole configurations are estimated as 20.4 Pa, 12.56 Pa, and 7.85 Pa respectively. Given that the measured yield shear stress of the HeLa cancer cell line is 13 Pa,[37] using the microfluidic dipole or quadrupole configurations at such flow rate could cause cell rupture. Note that since the maximum velocities are merely localized around the aspiration aperture (Fig. S1†), only very few cells that get isolated in close proximity to that area are exposed to such high shear stress.

Capture efficiency and cell viability

To evaluate the effect of MeFP's microfluidic multipoles configurations on the cell-capture efficiency, we experimentally characterize each configuration with HeLa cancer cells, and different flow rates while maintaining the same flow rates ratio. Capture efficiency is defined as the percentage ratio between the numbers of captured cells to the total injected cells under the MeFP. These experiments were carried out with injection to aspiration flow rates ratio of 3, tip-substrate gap of 40 μm and a 30 s application of 10 V pk–pk sinusoidal voltage of 10 MHz. As expected, across all flow rates, the overall capture efficiency increases with the number of aspiration apertures – upon reduction of the

average velocity of the flow stream and hence the viscous flow forces (Fig. 3a). For the microfluidic dipole configuration, the capture efficiency reduces from 92% with an injection flow rate of 0.5 μL min^{-1} to about 23% with a flow rate of 20 μL min^{-1}. The microfluidic heptapole configuration yields higher isolation efficiencies, approximately double that of the microfluidic dipole, at relatively high flow rates (>10 μL min^{-1}). Between 2.5 μL min^{-1} and 10 μL min^{-1}, the microfluidic heptapole configuration results in an average of 35% increase in capture efficiency in comparison to the dipole configuration. ESI† Video S1 shows cell isolation at the MeFP's micro-hump electrodes as the DEP force is turned ON and OFF while the injection flow rate is kept at 7.5 μL min^{-1} and flow rates ratio at 3.

Voltage is an independent adjustable parameter that can be used to improve isolation efficiencies at high flow rates. Using the microfluidic heptapole configuration, the isolation efficiency was improved by an average of 21% upon increasing the magnitude of the AC voltage to 30 V pk–pk (Fig. 3b). Applying high electric field strengths could adversely affect cell viability and physiology.[38,39] Hence, to deduce the upper limit of the applied voltage, cell viability studies were carried out for applied voltages ranging from 10–35 V pk–pk. For this range of voltages, the electric field strengths were estimated as 163–570 kV m^{-1}, respectively (Fig. S2†), which are within the range of DEP fields used for cell isolation in previous studies.[39] With voltages of up to 30 V pk–pk, very minimal cell death is recorded 24 hours after the isolation experiments hence, the percentage of viable cells does not significantly change even after 72 hours. (Fig. 3c). Cell proliferation rates after applying these voltages is also comparable to the controls (Fig. 3d). However, based on the principle of Joule heating, it must be noted that increased voltages result in increased temperatures (Fig. S3†) and long-term exposure of mammalian cells to elevated temperatures (>37 °C) could impose stresses on them.[40,41] In

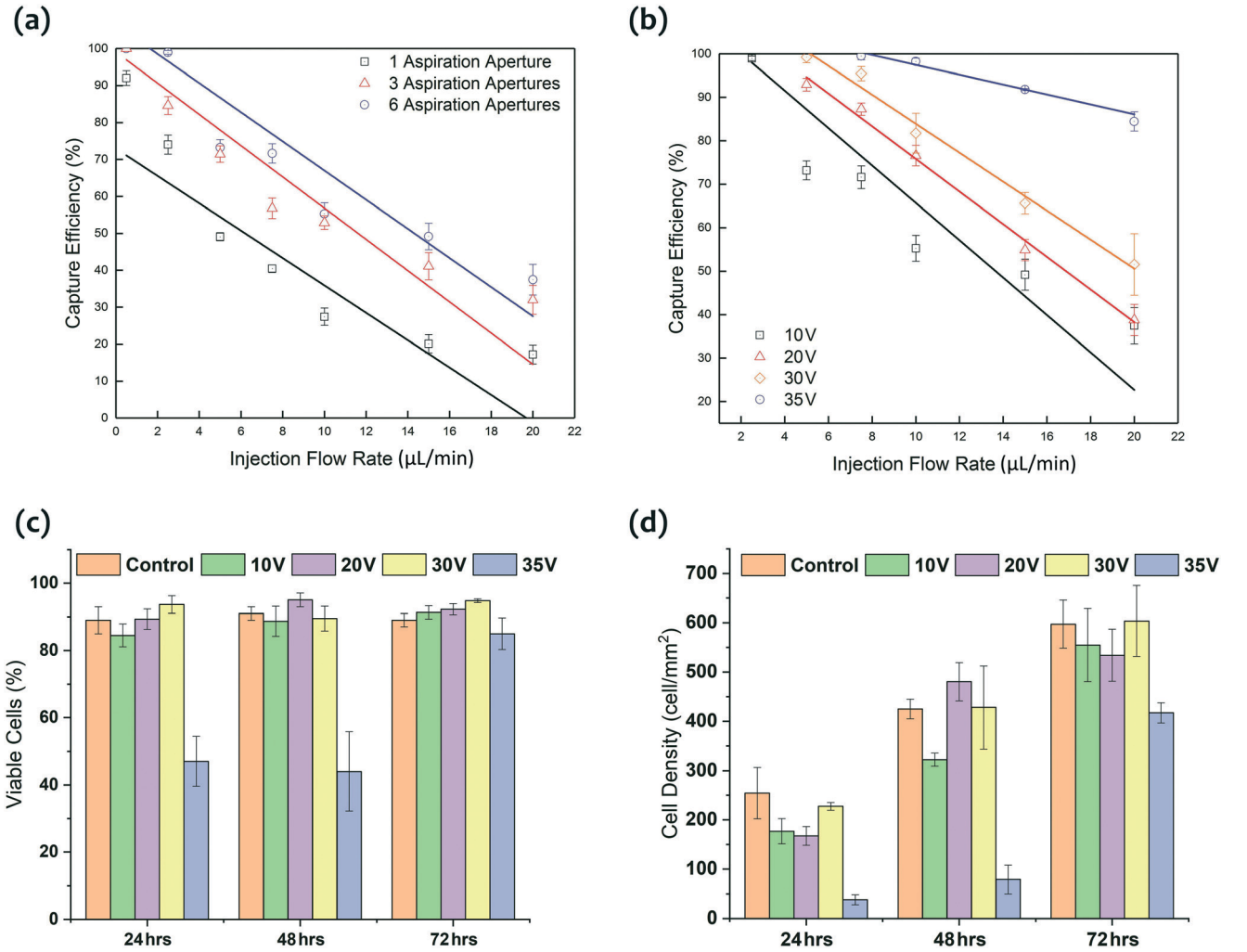

Fig. 3 Capture efficiency and cell viability. (a) Capture efficiency of HeLa cells as a function of injection flow rate and aperture configurations. Flow rates ratio is 3. (b) Capture efficiency of the MeFP microfluidic heptapole configuration as a function of injection flow rate and AC voltage magnitude while keeping the flow rates ratio at 3. (c) Percentage of viable cells cultured after exposing with varying AC voltage magnitudes. (d) Density of cultured cells after exposing with varying AC voltage magnitudes. Error bars indicate standard error of measurements from at least 3 separate experiments.

the present study, HeLa cells maintain acceptable viability at 30 V, with a maximum temperature of the 43.3 °C after 30 s exposure to the DEP forces (see Fig. S3†). While this can be attributed to the short exposure to elevated temperatures – the maximum temperature after 20 s is still about 38.9 °C – care must be taken in applying such electric field strengths on mammalian cells. Other conditions that could negatively influence viability or proliferation include the 3D printer resin, suspending cells in a low conductivity media, and culturing cells on an ITO coated substrate. Control experiments were used to investigate possible consequences of these factors and negligible effects were observed (Fig. S4†).

Capture efficiencies can be further improved by increasing the voltage to 35 V (Fig. 3b), however, we observed that this voltage generate bubbles in the dish (attributed to the poor electrochemical stability of the ITO electrodes at high voltages) and results in a 42% drop in percentage of viable cell recorded after 24 hours (Fig. 3c). Due to the shock induced on the cells at 35 V, their recovery period is longer hence, there is no observable change in percentage of viable cells between 24 and 48 hours (Fig. S5†). However, there is a significant increase in percentage of viable cells at 72 hours and this can be attributed to proliferation of cells that survived.

Cell separation

DEP enabled cell separation can be achieved by operating within an AC frequency window where one cell type undergoes repulsion through negative DEP while the other is attracted to the electrodes by positive DEP.[42] To utilize this technique, the frequency at which each cell types transition from positive to negative DEP (known as cross-over frequency) has to be determined. From eqn (1), this can be described as the AC frequency at which the CM function transitions from a positive to a negative value. Experimental characterization with the conventional co-planar interdigitated electrodes was used to determine the cross-

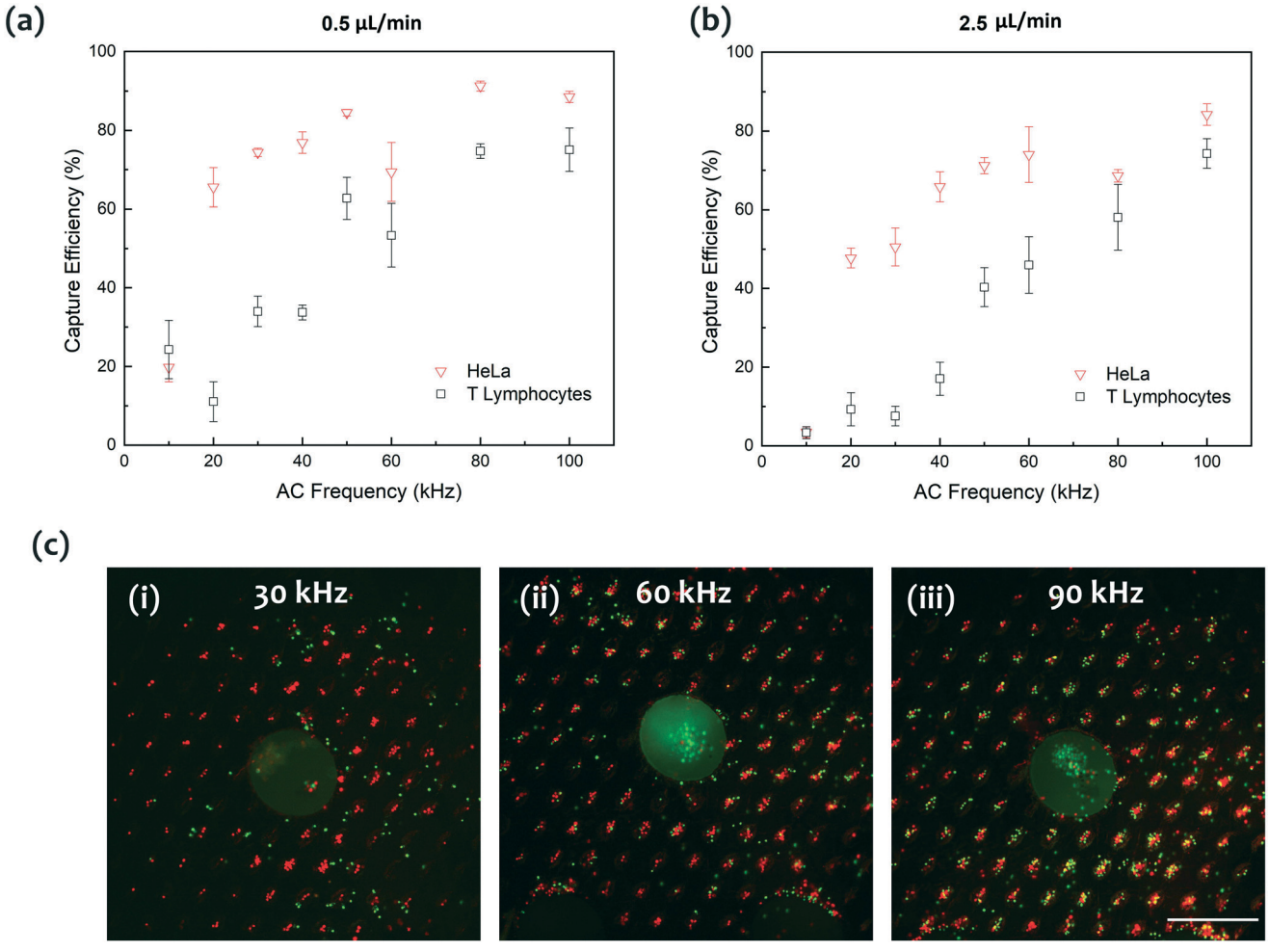

Fig. 4 MeFP cell separation. (a) Capture efficiency as a function of AC frequency for HeLa cells and T-lymphocytes at an injection flow rate of 0.5 μL min^{-1}. (b) Capture efficiency as a function of AC frequency for HeLa cells and T-lymphocytes at an injection flow rate of 2.5 μL min^{-1}. Flow rates ratio = 3. Error bars represent standard error of measurements from at least 3 separate experiments. Cell concentrations and applied voltage are 2 × 10^5 cell per mL of DEP buffer and 5 V, respectively. (c) Fluorescent images showing capture of HeLa (red) and T-lymphocytes (green) after 30 seconds of flow with AC frequencies of (i) 30 kHz, (ii) 60 kHz, and (iii) 90 kHz. Scale bar is 250 μm.

over frequencies of 10 ± 5 kHz, 15 ± 5 kHz and 35 ± 5 kHz for MCF-7, HeLa and T-lymphocyte cells respectively (see ESI† Video S2). Based on this, MATLAB modelling was used to visualize the frequency response of their CM factors (see Fig. S6†) and hence deduce a frequency of 30 kHz as an applicable separation parameter – where T-lymphocyte is in the negative DEP regime and HeLa/MCF-7 are in the positive DEP regime. In order to examine the applicability of the MeFP for separating cells based on this principle, we prepared a suspension with equal concentration of HeLa cells and T-lymphocytes, and characterized isolation efficiencies as a function of injection flow rate and AC frequency.

Using the microfluidic heptapole configuration, and an injection flow rate of 0.5 μL min^{-1} (flow rates ratio = 3), the isolation efficiencies of both HeLa and T-lymphocyte cells reduce as the frequency of the sinusoidal waveform is reduced from 100 kHz to 10 kHz (Fig. 4a). In addition, the capture efficiencies of T-lymphocytes (12.4 μm measured diameter) are lower than that of HeLa (17.1 μm measured diameter) across all frequencies. These results are expected following the theoretical formulation described in eqn (1). The magnitude of the DEP force is directly proportional to the frequency dependent CM factor, and cell size (r^3), whereas the direction of the force is only dependent on the CM factor.[24] However, while operating the MeFP at a flow rate of 0.5 μL min^{-1} (Fig. 4a), the capture efficiency of HeLa and T-lymphocytes around their respective cross-over frequencies are still about 20% and 34%, respectively. These

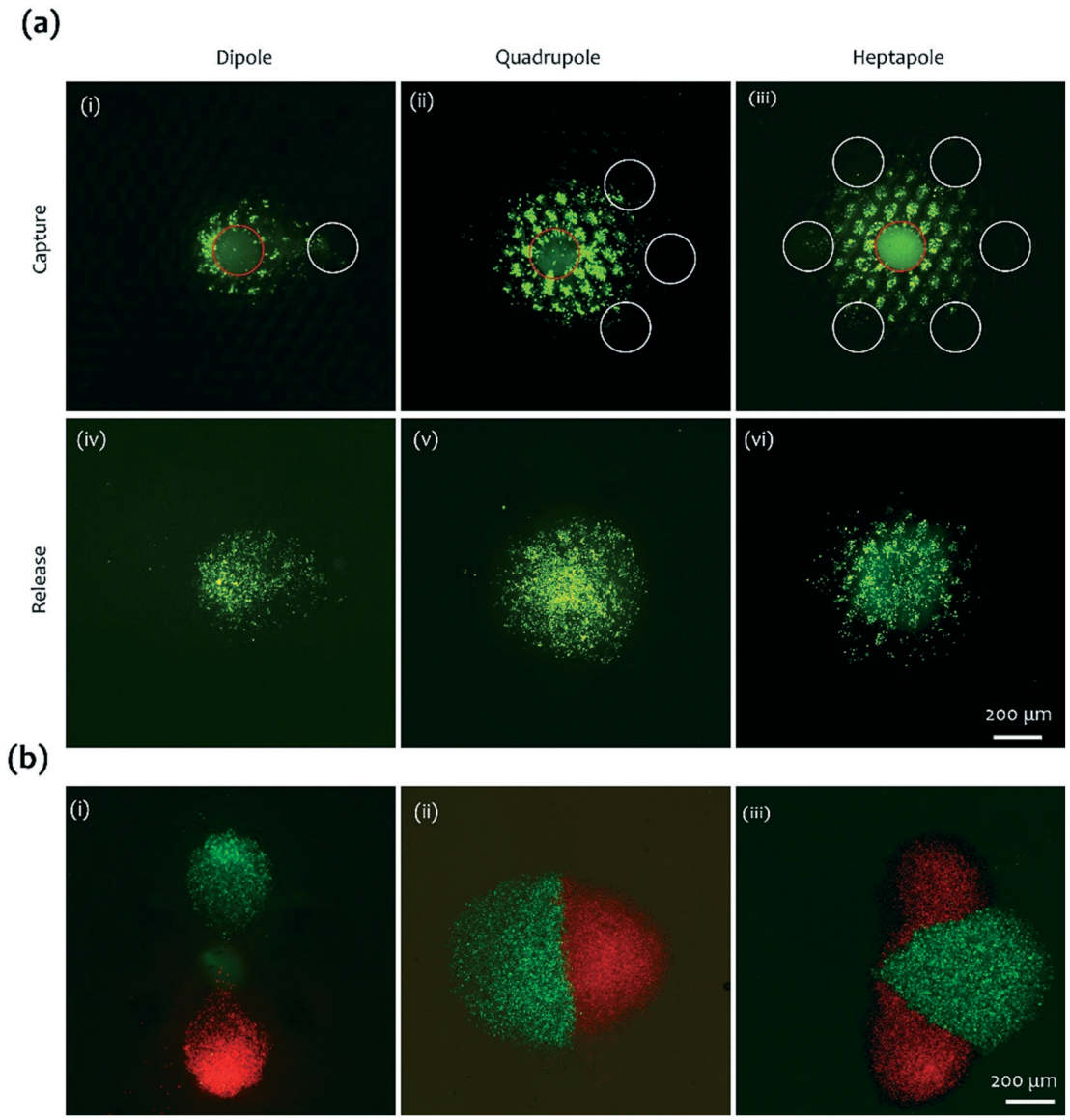

Fig. 5 MeFP cell patterning and co-cultures formation. (a) Fluorescent image of the isolated and released HeLa cells with microfluidic: (i) and (iv) dipole; (ii) and (v) quadrupole; (iii) and (vi) heptapole MeFP configurations. Red circle indicates injection aperture and white circle indicates aspiration aperture. (b) Co-culture patterns of HeLa (red) and MCF-7 (green) with (i) limited co-culture contact of two cell types, (ii) considerable co-culture contact of two cell types, and (iii) considerable co-culture contact of three cell types.

relatively high capture efficiencies at the cross-over frequencies can be attributed to the increased propensity of the cells to settle at very low flow rates, thus unfavorably contributing to the decreased capture purity. Capture purity is defined as the percentage ratio of the number of captured cells of interest to the number of total captured cells. Increasing the flow rate to 2.5 μL min^{-1} improves the capture purity (Fig. 4b), with best purity shown at the frequency of 30 kHz (in-between the ~15 kHz and 35 kHz cross-over frequencies of HeLa cells and T-lymphocytes, respectively). The 30 kHz frequency achieved up to 89.6% purity of HeLa cells, which evidently betters the 60.2% and 55.9% purities achieved at 60 and 90 kHz, respectively (Fig. 4c). While the maximum achieved purity does not represent perfect separation, it is in the range of previously reported values on the separation of T-lymphocytes using DEP.[43]

Cell patterning and co-cultures formation

After cell separation and washing out of non-target cells, captured target cells can be directly deposited on the glass slide by turning off the DEP forces. This is useful in reproducing complex cellular architectures *in vitro*, in the absence of closed conduits. Using the MeFP, HeLa cells are captured on the micro-hump electrodes in patterns that take the shape of the HFC and this shape is maintained after release onto the glass substrate (Fig. 5a). The deposited patterns of the microfluidic dipole, quadrupole and heptapole configuration visually match the numerically calculated profiles presented in Fig. 1b. To demonstrate the application of the MeFP for producing multiple cells co-culture patterns, suspensions of HeLa and MCF-7 (16.8 μm measured diameter and 10 ± 5 kHz cross-over frequency) cancer cell lines were adapted. By using these multicellular suspension streams, co-cultures with varying levels of co-culture contact can be produced – from limited culture–culture contact of two cell types (Fig. 5b (i)) to considerable co-culture contact of two cell types (Fig. 5b (ii)) and considerable co-culture contacts of three cell types (Fig. 5b (iii)). Using the same MeFP, several microfluidic multipoles configurations can be dynamically produced for complex cell co-culture architectures. Furthermore, a particularly unique feature of the MeFP lay in its ability to scan over the substrate to successively produce micro patterns or co-cultures at any location of interest within the substrate. To demonstrate this feature, upon release of the isolated cells, the MeFP is slowly withdrawn until a tip-substrate gap of about 5 mm is attained, and then moved to another location to repeat the cell deposition process – in about 2 minutes (see ESI† Video S3).

Discussions

This work presents the development of the DEP enabled MeFP as an open microfluidic tool for sequentially separating and patterning mammalian cells. Fabrication of the MeFP using 3D printing allows for a straightforward integration of the micro-hump electrodes which is a shape that facilitates generation of the required non-uniform electrical field. Using conventional fabrication techniques, this integration would have required very complicated, costly and time consuming procedures. An intuitive alternative would be to pattern the ITO glass slide to contain both DEP electrodes however, this also entail relatively high cost and complex procedures. Hence, this work buttresses 3D printing as a low cost, simple and flexible approach for developing new microfluidic technologies that were previously considered unfeasible to fabricate.

By coupling the gold coated MeFP with an ITO-coated glass slide, we demonstrate a pin-plate electrode configuration that introduces DEP forces within the HFC in order to selectively capture cells out of the flow stream between the injection and aspiration apertures. Based on the DEP principle, target cells are captured out of a stream of multiple cells using polarization (AC frequency dependent) discrimination. Hence, in a mixture of HeLa and T-lymphocytes, when operating at frequencies lower than the cross over frequency of T-lymphocytes (but higher than that of HeLa), HeLa is isolated on the tip of the electrodes by positive DEP, while T-lymphocytes continues flowing to the outlet. Subsequently, upon switching off the DEP force and the fluid flow, HeLa enriched on the electrodes is released by gravity to the bottom substrate. Since the cells are captured in a pattern that matches the HFC, in the absence of any disturbance, these cells settle on the glass slide in the same pattern. As such, using this setup, specific cell types can be efficiently enriched from a heterogeneous cell population, and consequently deposited on a flat substrate, in any pattern and any area of interest.

Characterization of the cell-capture feature of the MeFP, using numerical and experimental examinations, showed that increasing the number of aspiration apertures result in a reduction of the counteracting drag forces and hence increased capture efficiencies. Increasing the AC voltage magnitude is an alternative approach for improving capture efficiencies but cell culture studies revealed a maximum limit of 30 V pk–pk for a reasonable post capture cell viability. Using the microfluidic heptapole configuration, proof-of-concepts were provided in the form of sequentially separation and deposition of live mammalian cancer cells in defined patterns. Co-cultures were used to demonstrate the tools' capacity to produce variable patterns and operate in a scanning mode.

The MeFP provides improved engineering-control of cell co-culture environment for cell–cell interaction studies. For example, the device is applicable for studying hepatocyte-fibroblast interaction in co-cultures, which is a critical step for stabilizing liver specific functions *in vitro*.[44] In addition, since the MeFP construct co-cultures on an open and flat substrate (in absence of narrow channels), nutrient exchange during incubation is more effective. The device also has a potential application in the sequential capture and analysis of circulating tumor cells (CTCs). Since the MeFP can directly deposit captured CTCs on a flat glass substrate, cells can be

subsequently tested with multiple chemotherapeutic drugs using only the injection-aspiration feature of the same device. The open setup also permits transfer of the substrate containing the captured CTCs to mechanical characterization devices such as the atomic force microscope. Furthermore, by taking advantage of the scanning capability of the MeFP, multiple constructs can be produced on the same culture substrate, with spatial controllability, and without the requirement of any physical barrier.

The MeFP however has some drawbacks. The requirement of a conductive bottom substrate limits the versatility of the device. However, this can be overcome by sputtering gold on the electrodes in a pattern that ensure both electrical terminals are located on the MeFP. In addition, since the minimum size of the patterned constructs is limited by the channel diameter and spacing, low cost stereolithography 3D printers (>200 μm channel resolution) cannot be used to fabricate devices for highly miniaturized patterns (<500 μm total size). This also restricts the minimum spacing between multiple patterns. High-end 2-photon polymerization 3D printers like the Nanoscribe[45] will have to be adopted for more miniaturized constructs and higher spacing resolutions. Such printers could also open the way for the MeFP as a single cell manipulation and/or stimulation tool *e.g.* single cell tweezing or electroporation.[46,47]

Overall, we believe the MeFP is a multifunctional tool for manipulating cells in open space and this demonstration of its simple, dynamic and customizable nature will inspire new life science applications.

Author contribution

The study was conceptualized and designed by A. B. and M. A. Q. Research was carried by A. B. and A. M. The manuscript was written by A. B., A. M., and M. A. Q.

Conflicts of interest

There are no conflicts of interest.

Acknowledgements

A. B. acknowledges NYUAD Global PhD Fellowship. This research was funded in part by the NYUAD Research Enhancement Fund (REF 2017, New York University Abu Dhabi), the ADEK Excellence Award from Abu Dhabi Department of Education and Knowledge, Abu Dhabi, UAE, and Seed Grants (AJF201523 and AJF2018085) from Al Jalila Foundation, Dubai, UAE. The authors acknowledge technical support from the NYUAD Core Technology Platforms.

References

1 R. K. Kumar and A. W. J. Lykke, Cell separation: A review, *Pathology*, 1984, **16**, 53–62.
2 W. Al-Faqheri, T. H. G. Thio, M. A. Qasaimeh, A. Dietzel, M. Madou and A. Al-Halhouli, Particle/cell separation on microfluidic platforms based on centrifugation effect: a review, *Microfluid. Nanofluid.*, 2017, **21**, 102.
3 A. Vembadi, A. Menachery and M. A. Qasaimeh, Cell Cytometry: Review and Perspective on Biotechnological Advances, *Front. Bioeng. Biotechnol.*, 2019, **7**, 147.
4 J. He, A. T. Brimmo, M. A. Qasaimeh, P. Chen and W. Chen, Recent Advances and Perspectives in Microfluidics-Based Single-Cell Biosensing Techniques, *Small Methods*, 2017, **1**, 1700192.
5 A. Rosenthal, A. Macdonald and J. Voldman, Cell patterning chip for controlling the stem cell microenvironment, *Biomaterials*, 2007, **28**, 3208–3216.
6 C. Kuo Te, J. Y. Wang, A. M. Wo, B. P. C. Chen and H. Lee, ParaStamp and Its Applications to Cell Patterning, Drug Synergy Screening, and Rewritable Devices for Droplet Storage, *Adv. Biosyst.*, 2017, **1**, 1700048.
7 C. T. Ho, R. Z. Lin, W. Y. Chang, H. Y. Chang and C. H. Liu, Rapid heterogeneous liver-cell on-chip patterning via the enhanced field-induced dielectrophoresis trap, *Lab Chip*, 2006, **6**, 724–734.
8 H. Kaji, G. Camci-Unal, R. Langer and A. Khademhosseini, Engineering systems for the generation of patterned co-cultures for controlling cell-cell interactions, *Biochim. Biophys. Acta, Gen. Subj.*, 1810, **2011**, 239–250.
9 B. Guillotin and F. Guillemot, Cell patterning technologies for organotypic tissue fabrication, *Trends Biotechnol.*, 2011, **29**, 183–190.
10 S. R. Khetani and S. N. Bhatia, Microscale culture of human liver cells for drug development, *Nat. Biotechnol.*, 2008, **26**, 120–126.
11 S. N. Bhatia, U. J. Balis, M. L. Yarmush and M. Toner, Effect of cell-cell interactions in preservation of cellular phenotype: Cocultivation of hepatocytes and nonparenchymal cells, *FASEB J*, 1999, **13**, 1883–1900.
12 A. J. Engler, P. O. Humbert, B. Wehrle-Haller and V. M. Weaver, Multiscale modeling of form and function, *Science*, 2009, **324**, 208–212.
13 C. M. Nelson and J. Tien, Microstructured extracellular matrices in tissue engineering and development, *Curr. Opin. Biotechnol.*, 2006, **17**, 518–523.
14 F. Goulet, C. Normand and O. Morin, Cellular interactions promote tissue-specific function, biomatrix deposition and junctional communication of primary cultured hepatocytes, *Hepatology*, 1988, **8**, 1010–1018.
15 O. Morin and C. Normand, Long-term maintenance of hepatocyte functional activity in co-culture: Requirements for sinusoidal endothelial cells and dexamethasone, *J. Cell. Physiol.*, 1986, **129**, 103–110.
16 N. Pamme, Magnetism and microfluidics, *Lab Chip*, 2006, **6**, 24–38.
17 A. Ashkin, History of optical trapping and manipulation of small-neutral particle, atoms, and molecules, *IEEE J. Sel. Top. Quantum Electron.*, 2000, **6**, 841–856.
18 A. Shenoy, C. V. Rao and C. M. Schroeder, Stokes trap for multiplexed particle manipulation and assembly using fluidics, *Proc. Natl. Acad. Sci. U. S. A.*, 2016, **113**, 3976–3981.

19 M. Dyson, B. Woodward and J. B. Pond, Flow of red blood cells stopped by ultrasound [23], *Nature*, 1971, **232**, 572–573.
20 N. V. Baker, Segregation and sedimentation of red blood cells in ultrasonic standing waves, *Nature*, 1972, **239**, 398–399.
21 R. Z. Lin, C. T. Ho, C. H. Liu and H. Y. Chang, Dielectrophoresis based-cell patterning for tissue engineering, *Biotechnol. J.*, 2006, **1**, 949–957.
22 A. Rosenthal and J. Voldman, Dielectrophoretic traps for single-particle patterning, *Biophys. J.*, 2005, **88**, 2193–2205.
23 H. A. Pohl, *Dielectrophoresis*, Cambridge University Press, Cambridge, Engl 1978; : 495.
24 R. Pethig, Dielectrophoresis, Status of the theory, technology and applications, *Biomicrofluidics*, 2010, **4**, 22811.
25 Z. R. Gagnon, Cellular dielectrophoresis: Applications to the characterization, manipulation, separation and patterning of cells, *Electrophoresis*, 2011, **32**, 2466–2487.
26 D. Juncker, H. Schmid and E. Delamarche, Multipurpose microfluidic probe, *Nat. Mater.*, 2005, **4**, 622–627.
27 M. A. Qasaimeh, T. Gervais and D. Juncker, Microfluidic quadrupole and floating concentration gradient, *Nat. Commun.*, 2011, **2**, 464.
28 P. A. Goyette, É. Boulais, F. Normandeau, G. Laberge, D. Juncker and T. Gervais, Microfluidic multipoles theory and applications, *Nat. Commun.*, 2019, **10**, 1781.
29 M. Safavieh, M. A. Qasaimeh, A. Vakil, D. Juncker and T. Gervais, Two-aperture microfluidic probes as flow dipole: Theory and applications, *Sci. Rep.*, 2015, **5**, 11943.
30 A. Brimmo, P. A. Goyette, R. Alnemari, T. Gervais and M. A. Qasaimeh, 3D Printed Microfluidic Probes, *Sci. Rep.*, 2018, **8**, 10995.
31 G. H. Czerlinski, D. S. Reid, A. Apostol, K. D. Bauer and D. G. Scarpelli, Determination of the density of cells from sedimentation studies at 1G, *J. Biol. Phys.*, 1987, **15**, 29–32.
32 A. J. Goldman, R. G. Cox and H. Brenner, Slow viscous motion of a sphere parallel to a plane wall-II Couette flow, *Chem. Eng. Sci.*, 1967, **22**, 653–660.
33 M. P. Hughes, *Nanoelectromechanics in engineering and biology*, CRC press, 2002, DOI: 10.1201/9781315219202.
34 H. Morgan and N. G. Green, *AC electrokinetics: colloids and nanoparticles, Microtechnologies Microsystems Ser.*, 2002, vol. 2, 326.
35 G. G. Stokes, On the Effect of the Internal Friction of Fluids on the Motion of Pendulums, *Math. Phys. Pap.*, 2010, **9**, 1–10.
36 W. H. Grover, A. K. Bryan, M. Diez-Silva, S. Suresh, J. M. Higgins and S. R. Manalis, Measuring single-cell density, *Int. Conf. Miniaturized Syst. Chem. Life Sci., 15th*, 2011, **2011**(1), 6–8.
37 Y. Shi, D. D. Y. Ryu and R. Ballica, Rheological properties of mammalian cell culture suspensions: Hybridoma and HeLa cell lines, *Biotechnol. Bioeng.*, 1993, **41**, 745–754.
38 S. P. Desai and J. Voldman, Measuring the impact of dielectrophoresis on cell physiology using a high-content screening platform, in: *12th International Conference on Miniaturized Systems for Chemistry and Life Sciences - The Proceedings of MicroTAS 2008 Conference*, 2008, pp. 1308–1310.
39 D. S. Gray, J. L. Tan, J. Voldman and C. S. Chen, Dielectrophoretic registration of living cells to a microelectrode array, *Biosens. Bioelectron.*, 2004, **19**, 771–780.
40 S. Varma, A. Fendyur, A. Box and J. Voldman, Multiplexed Cell-Based Sensors for Assessing the Impact of Engineered Systems and Methods on Cell Health, *Anal. Chem.*, 2017, **89**, 4663–4670.
41 S. Varma and J. Voldman, Caring for cells in microsystems: principles and practices of cell-safe device design and operation, *Lab Chip*, 2018, **18**, 3333–3352.
42 R. Pethig and G. H. Markx, Applications of dielectrophoresis in biotechnology, *Trends Biotechnol.*, 1997, **15**, 426–432.
43 X. B. Wang, J. Yang, Y. Huang, J. Vykoukal, F. F. Becker and P. R. C. Gascoyne, Cell separation by dielectrophoretic field-flow-fractionation, *Anal. Chem.*, 2000, **72**, 832–839.
44 S. N. Bhatia, M. L. Yarmush and M. Toner, Controlling cell interactions by micropatterning in co-cultures: Hepatocytes and 3T3 fibroblasts, *J. Biomed. Mater. Res.*, 1997, **34**, 189–199.
45 F. Niesler and M. Hermatschweiler, Two-Photon Polymerization - A Versatile Microfabrication Tool: From maskless lithography to 3D printing, *Laser Tech. J.*, 2015, **12**, 44–47.
46 T. P. Hunt and R. M. Westervelt, Dielectrophoresis tweezers for single cell manipulation, *Biomed. Microdevices*, 2006, **8**, 227–230.
47 J. Olofsson, K. Nolkrantz, F. Ryttsén, B. A. Lambie, S. G. Weber and O. Orwar, Single-cell electroporation, *Curr. Opin. Biotechnol.*, 2003, **14**, 29–34.

Electronic Supplementary Material (ESI) for Lab on a Chip.

Supplementary Figures

Microelectrofluidic Probe for Sequential Cell Separation and Patterning

Ayoola T. Brimmo[1, 2], Anoop Menachery[1], Mohammad A. Qasaimeh[1,2]
[1]Division of Engineering, New York University Abu Dhabi
[2]Department of Mechanical and Aerospace Engineering, New York University, New York

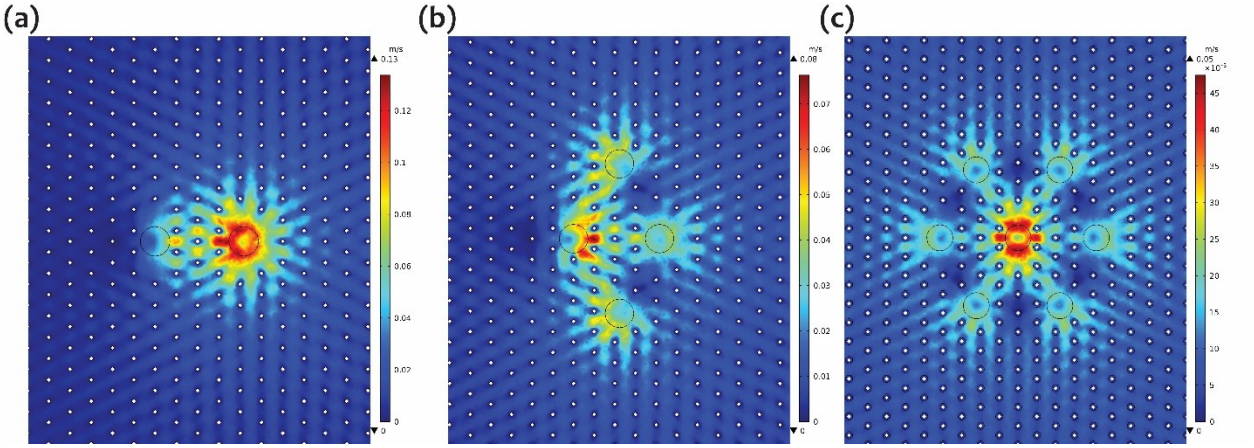

Fig. S1. Velocity profile at capture plane with 20 µl/min inlet flow rate. (a) Dipole Microfluidic configuration. (b) Quadrupole Microfluidic configuration. (c) Heptapole Microfluidic configuration.

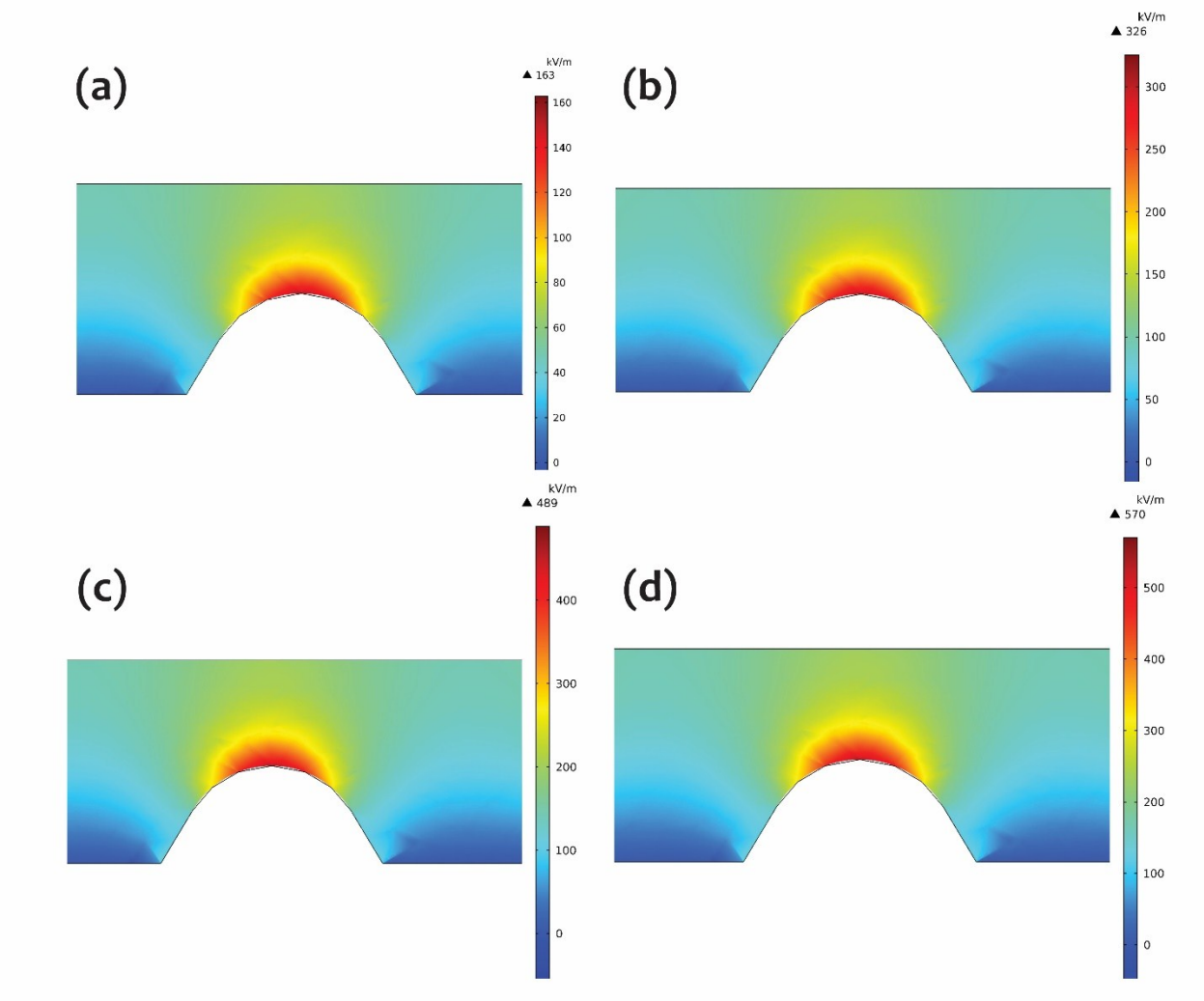

Fig. S2. Electric field strength as a function applied voltage. (a) 10 Vpk-pk. (b) 20 Vpk-pk. (c) 30V pk-pk. (d) 40 Vpk-pk.

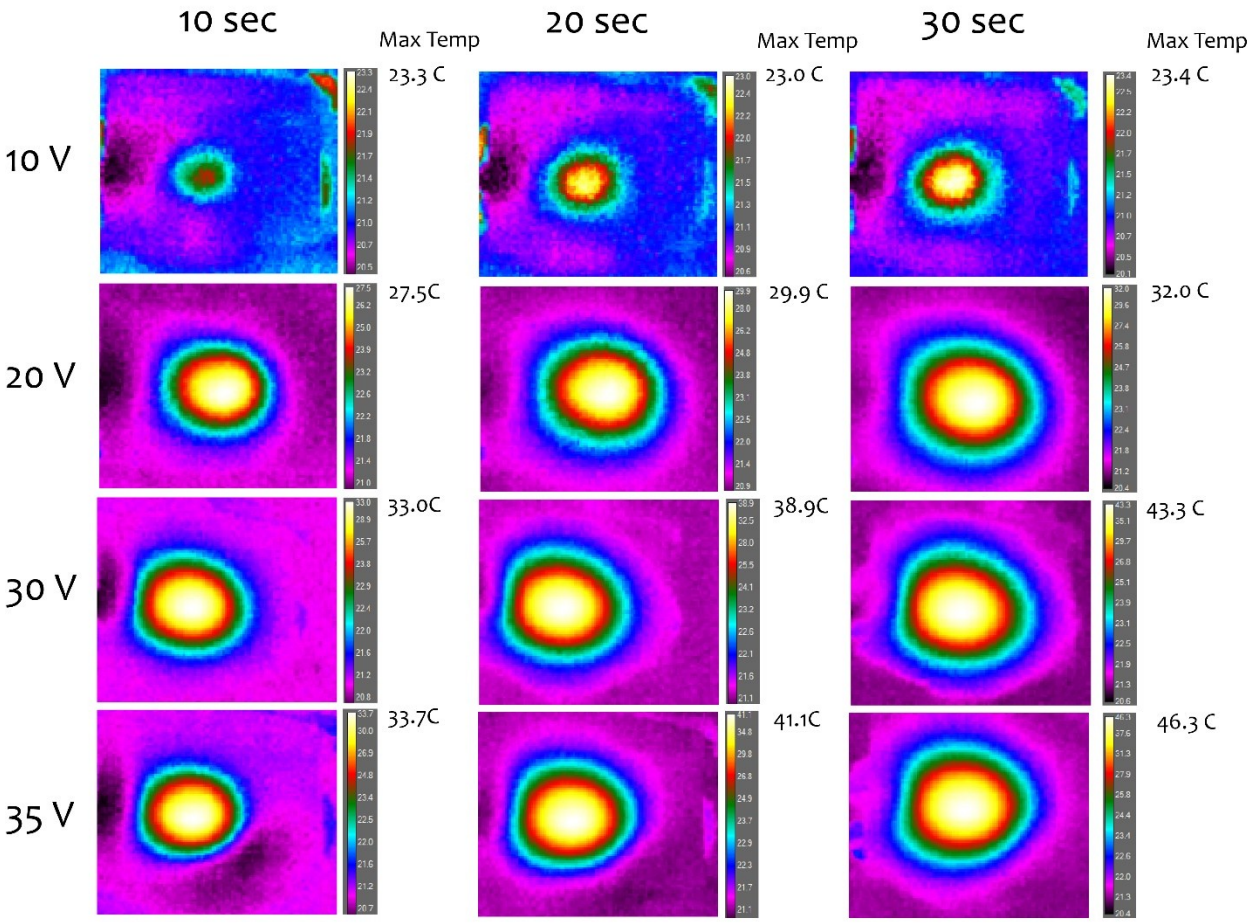

Fig. S3. Temperature measurements as a function of applied voltage and exposure time. Transient Infrared images as a function of applied voltage showed that the maximum temperature cells were exposed to at 35 V is 46.3 C

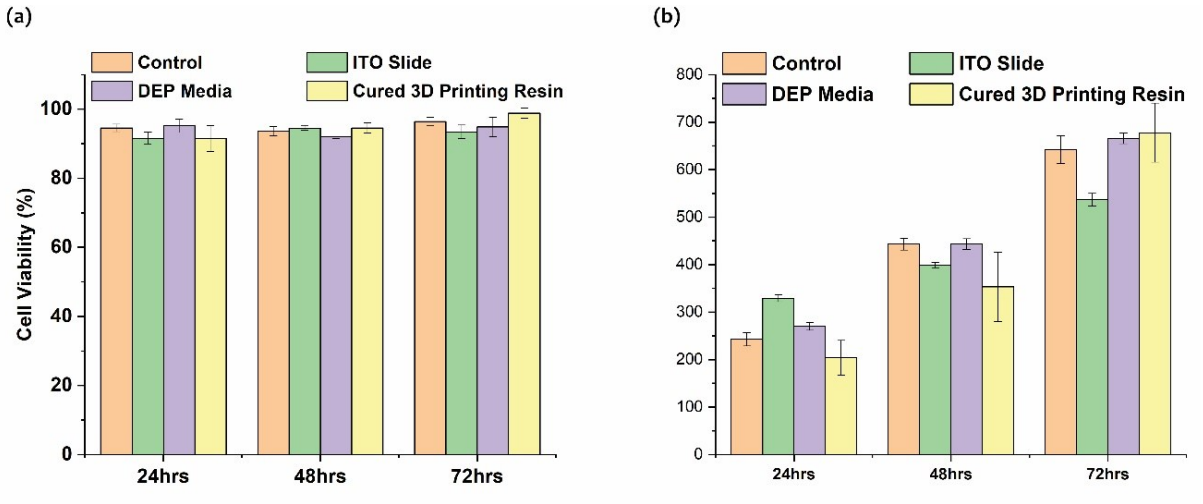

Fig. S4. Impact of materials on cell viability and growth density. (a) Cell viability as a function of time for different materials used in the study. (b) Cell density as a function of time for different materials used in the study. Error bars denote standard error.

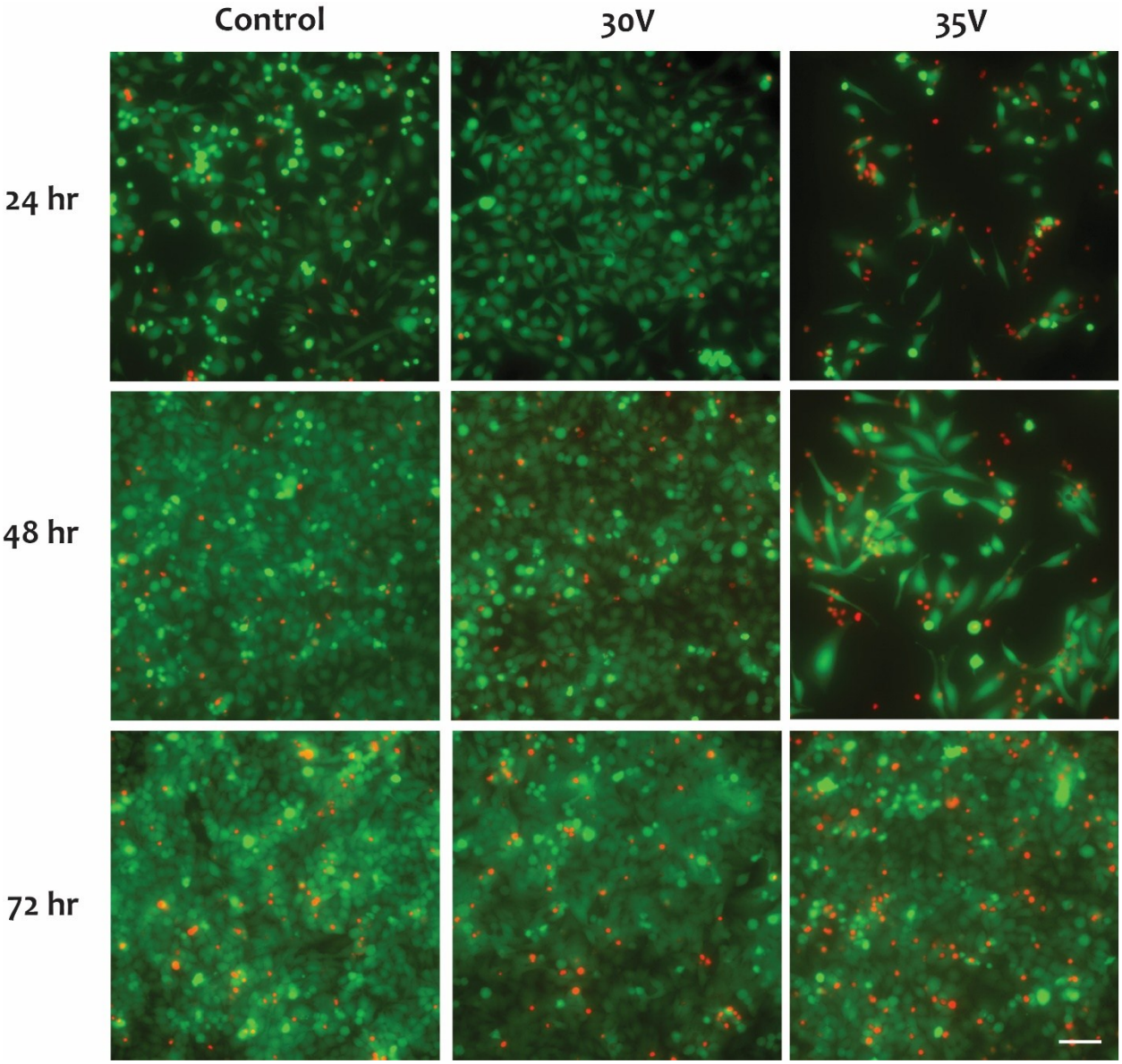

Fig. S5. Fluorescent image for live/dead viability study. Green denotes live cells and red denotes dead cells. Scale bar is 100 µm.

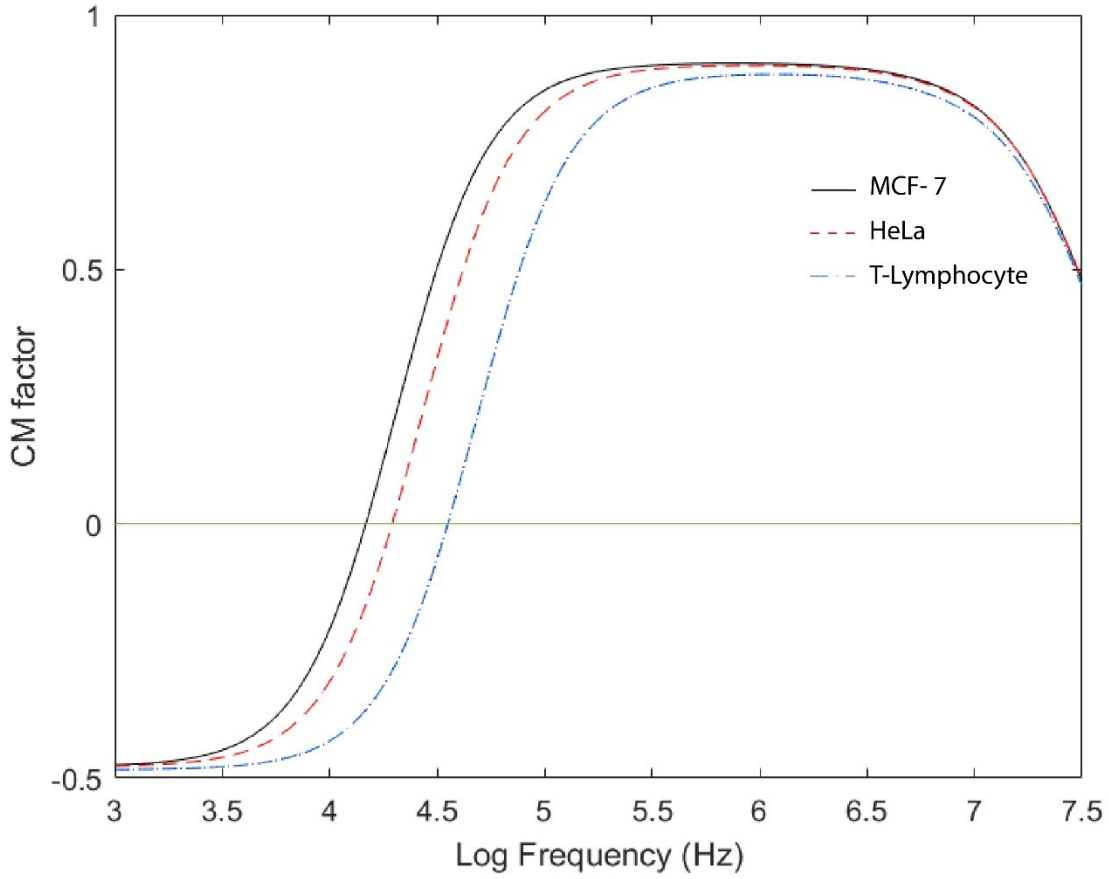

Fig. S6. Calculated CM function of MCF 7, HeLa, and T-lymphocytes. Frequency dependent CM-function calculated using the two-shelled model